Phase-sensitive detection for unconventional Bose-Einstein condensation

Zi Cai,[1] Lu-Ming Duan,[2,3] and Congjun Wu[1,3]

[1]*Department of Physics, University of California, San Diego, California 92093, USA*
[2]*Department of Physics and MCTP, University of Michigan, Ann Arbor, Michigan 48109, USA*
[3]*Center for Quantum Information, IIIS, Tsinghua University, Beijing, China*

We propose a phase-sensitive detection scheme to identify the unconventional $p_x \pm i p_y$ symmetry of the condensate wave functions of bosons, which have already been proposed and realized in high bands in optical lattices. Using the impulsive Raman operation combined with time-of-flight imaging, the off-diagonal correlation functions in momentum space give rise to the relative phase information between different components of condensate wave functions. This scheme is robust against the interaction and interband effects, and provides evidence of unconventional Bose-Einstein condensations with nontrivial condensation symmetries.

Macroscopic condensates of bosons and paired fermions are of central interest in condensed-matter physics. Order parameters of Cooper pairings are termed "unconventional" if they belong to nontrivial representations of rotational symmetry groups. Celebrated examples include the d-wave pairing states of high-T_c cuprates [1,2], the p-wave pairing states of ^{3}He A and B phases [3], and Sr$_2$RuO$_4$ [4,5]. Among various experimental tools, phase-sensitive detections are exceptional as they provide evidence of unconventional pairing symmetries, such as the π-phase shifts in the joint-corner superconducting quantum interference device (SQUID) junctions [1] and the tri-crystal superconducting ring experiments [2] of high-T_c cuprates. Unconventional symmetries have also been generalized to the particle-hole channel pairings, i.e., the Pomeranchuk-type Fermi surface instabilities. The spin instabilities in high orbital angular momentum channels are denoted as "unconventional magnetism."

Recently, unconventional symmetries have been introduced to the single-boson condensates [6,7], denoted as "unconventional" Bose-Einstein condensations (UBECs). Their condensate wave functions belong to nontrivial representations of the lattice point group. Such states have been proposed in high orbital bands of optical lattices [8–14]. These systems have been experimentally realized by pumping bosons into high orbital bands [15–17]. Bosons have been observed to develop phase coherence before they decay to the lowest band. In addition, in the artificial lattice systems of exciton-polariton in semiconductor quantum wells, a d-wave condensation in the excited bands of bosons have also been observed [18]. These UBECs are beyond Feynman's "no-node" theorem [6,19], which states that the ground-state wave functions of bosons are positive-definite under very general circumstances. This theorem applies to the system of superfluid ^{4}He [19] and many experiments of alkali bosons [20]. It also implies that time-reversal (TR) symmetry cannot be spontaneously broken in usual BECs. However, UBECs, which are metastable excited states of bosons instead of the ground state, escape from the "no-node" constraint. Their condensate wave functions are nodal, which are able to break TR symmetry spontaneously under certain conditions [6].

The recent UBECs realized in Hemmerich's group is an exciting progress [16], where the time-of-flight (TOF) spectrum has revealed signatures of both the real and complex UBECs by tuning the anisotropy of the optical lattice. However, the TOF images can only provide the single-particle density distribution in momentum space; thus in the complex UBECs, the key information about the relative phase between the condensate components is lost during TOF. Without the phase information, the TOF images of the $p_x \pm i p_y$ BEC can be interpreted by other plausible scenarios such as the phase separation between two real condensates at different momenta or the incoherent mixing between them [21]. It would be important to have evidence of the phase difference $\pm\frac{\pi}{2}$ between the two condensate components.

In this paper, we propose a phase-sensitive detection scheme to identify the $p_x \pm i p_y$ symmetry of UBECs by measuring the relative phases of $\pm\frac{\pi}{2}$. This proposal is based on the scheme in Ref. [22], which has been used to construct the off-diagonal correlation functions in momentum space for UBECs. By implementing a momentum-kick Raman pulse, we build up the connection between bosons with different condensate momenta in the complex UBEC. The off-diagonal order of BEC has also been measured by the Bragg spectrum [23,24]. As we will show below, the relative phase information is uniquely tied to the off-diagonal correlations between the different condensate momenta, which can be measured in time-of-flight imaging through the impulsive Raman pulse. We note that a different scheme was proposed recently by Kitagawa *et al.* for phase-sensitive detection of nontrivial pairing symmetries in ultracold fermions based on two-particle interferometry [25].

Our scheme is connected with the experiment in Ref. [16], where the bosons are pumped to the first excited band of a s-p hybridized system (hybridization between the s orbital of the shallow sublattice A and the p orbital of the deep sublattice B as illustrated in Fig. 1(a). Two degenerate band minima (denoted as $K_{1,2}$ below) locate at the lattice momenta $\frac{1}{2}\vec{b}_{1,2}$ with $\vec{b}_{1,2} = (\pm\pi, \pi)$ the reciprocal lattice vectors (we set the lattice constant $a = 1$), as shown in Fig. 1(b). Bloch-wave states $\Psi_{1,2}(\mathbf{r})$ at $K_{1,2}$ points are time-reversal invariant and can be expressed as $\Psi_{1,2}(\mathbf{r}) = e^{iK_{1,2}\mathbf{r}}u_{K_{1,2}}(\mathbf{r})$, where $u_{K_{1,2}}(\mathbf{r})$ are periodic wave functions and can been obtained by energy band calculation [7]. The complex combination of $\Psi_\pm = (\Psi_1 \pm i\Psi_2)/\sqrt{2}$ only have nodal points from intersections
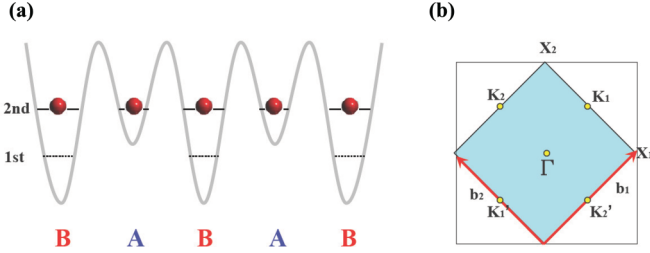
(a)

(b)

FIG. 1. (Color online) (a) Bipartite lattice structure (along the x direction) in Hemmerich's experiment [16], where bosons are loaded into the second band. (b) First Brillouin zone (blue area) and basis vectors of the reciprocal lattice $\vec{b}_{1,2}$.

FIG. 2. (Color online) Using two Raman pulses with different propagating directions to build up the momentum transfer between bosons at K_1 and K_2.

of the nodal lines of $\Psi_{1,2}$. With repulsive interaction, the complex condensates $\Psi_\pm$ with nodal points are favored since their spatial distributions of particle density are more uniform and extensive than other states, minimizing the interaction energy [7].

Both of the wave functions $\Psi_{1,2}(\mathbf{r})$ have odd parity with the p-wave symmetry. Rigorously speaking, the lattice configuration in Ref. [16] does not have four-fold rotational symmetry, and thus $\Psi_{1,2}$ are not transformable to each other by the rotation of $90°$. Nevertheless, for simplicity, we still denote these condensates with the $p_x \pm i p_y$ symmetry. The TOF imaging in the experiment [16] has observed four peaks at $(K_{1,2}, K'_{1,2} \equiv K_{1,2} - \vec{b}_{1,2})$ with the same height, which implies that the condensate has two equal weights of the Ψ_1 and Ψ_2. However, the phase difference between the two components Ψ_1 and Ψ_2, which is critical for verifying the novel $p_x \pm i p_y$ condensation symmetry, is not clear.

The spirit of our proposal for the phase-sensitive detection can be outlined as follows: for the condensate $|\Psi_c\rangle = \frac{1}{2^{N_0/2}\sqrt{N_c!}}(C^\dagger_{K_1} + e^{i\theta}C^\dagger_{K_2})^{N_c}|O\rangle$, where N_c is the boson number in the condensate, $C^\dagger_{K_1}$ ($C^\dagger_{K_2}$) is the bosonic operator creating a boson at K_1 (K_2), and θ is the relative phase between bosons in K_1 and K_2. If $\theta \neq 0$ and π, the condensate exhibits a vortex-antivortex lattice structure. The staggered orbital angular momentum (OAM) density wave order parameter is defined as $L_z(\vec{Q}) = i(C^\dagger_{K_1}C_{K_2} - C^\dagger_{K_2}C_{K_1})$ where $\vec{Q} = \vec{K}_1 - \vec{K}_2$. Its magnitude reads as $\langle\Psi_c|L_z(\vec{Q})|\Psi_c\rangle = N_c\sin\theta$, which is just the off-diagonal correlation. It reaches maximum for the $p_x \pm i p_y$ state ($\theta = \pm\frac{1}{2}\pi$). If we implement a Raman operation to transform the bosons in the original condensate into [22]

$$C'_{K_1} = \frac{1}{\sqrt{2}}(C_{K_1} - iC_{K_2}), \quad C'_{K_2} = \frac{1}{\sqrt{2}}(C_{K_2} - iC_{K_1}), \quad (1)$$

we can measure the density difference of the new BECs $\delta n' \equiv \langle\Psi_C|C'^\dagger_{K_2}C'_{K_2} - C'^\dagger_{K_1}C'_{K_1}|\Psi_c\rangle$ through the TOF imaging. $\delta n'$ exactly gives the desired off-diagonal correlation as

$$\delta n' = i\langle\Psi_c|C^\dagger_{K_1}C_{K_2} - C^\dagger_{K_2}C_{K_1}|\Psi_c\rangle. \quad (2)$$

Now we turn back to Hemmerich's experiment and show how to implement the Raman transition. Similar to Ref. [22], the Raman transition can be realized by two traveling-wave laser beams propagating along different directions (as plotted in Fig. 2) with corresponding wave vector $\mathbf{k_{1,2}}$ and frequency
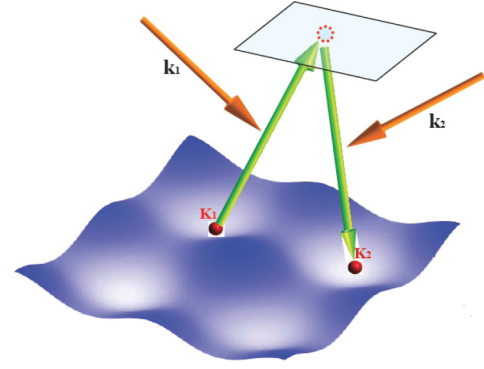
$\omega_{1,2}$, which introduce an effective Raman Rabi frequency with a spatially varying phase $\Omega(\mathbf{r},t) = \Omega_0 e^{i(\delta\mathbf{k}\cdot\mathbf{r}-\delta\omega t+\phi)}$, where $\delta\mathbf{k} = \mathbf{k_1} - \mathbf{k_2}$, $\delta\omega = \omega_1 - \omega_2$, and ϕ is the relative phase between the two Raman beams. Ω_0 is expressed as $\Omega_0 = \Omega_1\Omega_2^*/\Delta$, where Δ is the detuning, $\Omega_{1(2)}$ are the resonant Rabi frequencies for the individual transitions between the initial (final) states and the intermediate state and are proportional to the strength of the electric field of the corresponding Raman beams. This spatially dependent Raman transition builds up the connection between the condensation components in two degenerate points $K_{1,2} = (\pm\pi/2, \pi/2)$, which demands that $\delta\mathbf{k} = K_2 - K_1 = (\pi, 0)$. (Notice that $\delta\mathbf{k}$ and $-\delta\mathbf{k}$ are connected by a reciprocal lattice vector and thus equivalent. Because of this feature, the Raman scheme here is simpler than the one in Ref. [22] which needs to use a transition between two different hyperfine levels.) The effective Hamiltonian for the Raman process is described by

$$H_R = \int d\mathbf{r}\,\Omega(\mathbf{r},t)\Psi^\dagger(\mathbf{r})\Psi(\mathbf{r}) + \text{H.c.}, \quad (3)$$

which, together with the original atomic Hamiltonian H_0 in the optical lattice, gives the full Hamiltonian of the system [16].

Different from Ref. [22], in the experiment [16] the optical lattice is too shallow to apply the tight binding approximation. Instead, we expand the field operator in the Bloch representation as

$$\Psi(\mathbf{r}) = \sum_{n\mathbf{k}} C_{n\mathbf{k}}\psi_{n\mathbf{k}}(\mathbf{r}), \quad (4)$$

where $C_{n\mathbf{k}}$ is the bosonic operator annihilating a boson in the nth band with momentum $\mathbf{k}$, $\psi_{n\mathbf{k}}(\mathbf{r})$ is the Bloch wave function, and the summation of $\mathbf{k}$ is over the first Brillouin zone (BZ). We choose the effective Rabi frequency Ω_0 of the Raman pulse so that it is smaller than the band gap but larger than the atomic hopping rate in the lattice ($t \ll \hbar\Omega_0 \ll \Delta_{12}$). Under this condition, we can neglect the interband tunneling as well as the time dependence of the wave packets $\Psi_1(\mathbf{r})$ and $\Psi_2(\mathbf{r})$ during the Raman operation. For the typical values of the experiment parameters, the energy band structure is shown in Fig. 3. The hopping rate is estimated by $t \approx 0.05E_r \approx 2\pi\hbar \times 0.1$ kHz and the smallest band gap $\Delta_{12} \approx 1.08E_r \approx 2\pi\hbar \times 2.2$ kHz. If we choose $\hbar\Omega_0 \sim 2\pi\hbar \times 0.5$ kHz, the corrections to the above approximation, estimated by $t^2/(\hbar\Omega_0)^2$ and $(\hbar\Omega_0)^2/\Delta_{12}^2$, are
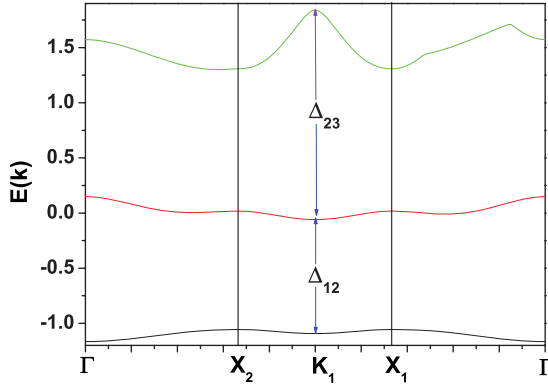
FIG. 3. (Color online) Energy spectra along the lines between the high symmetry points with the experimental values of the parameters given in Ref. [16].
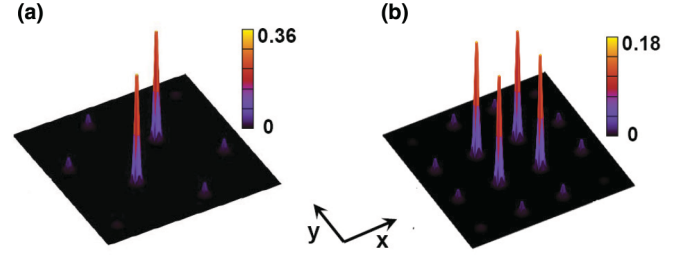

FIG. 4. (Color online) TOF imaging after the Raman transition with $\phi = 0$ for (a) the complex UBEC ($\Psi_1 + i\Psi_2$) and (b) incoherent mixing of the real UBECs (Ψ_1 and Ψ_2).

pretty small. In our case, the Raman operation induces a transition between the complex and polar BECs with the same kinetic energy but different interaction energy. $\hbar\delta\omega$ should match the energy difference between the initial (complex UBEC) and final (real UBEC) states of the Raman transition, which can be estimated as $10^{-3}E_r \approx 2\pi\hbar \times 2.1$ Hz and much smaller than $\hbar\Omega_0$. Therefore, the phase accumulation induced by $\delta\omega$ within the duration of Raman pulse δt can be neglected ($\delta\omega\delta t \ll \pi/4$), and the Raman Rabi frequency in Eq. (3) can be considered as time independent during the Raman transition.

Under the above approximations, H_R is simplified to

$$H_R = e^{i\phi} \sum_{\mathbf{k}} \Omega(\mathbf{k}) C^\dagger_{\mathbf{k}+\delta\mathbf{k}} C_{\mathbf{k}} + \text{H.c.}, \qquad (5)$$

which is constrained only to the relevant band. The summation of $\mathbf{k}$ is over the first BZ, and the effective Raman-Rabi frequency $\Omega(\mathbf{k})$ is $\mathbf{k}$ dependent and can be calculated based on the eigenvectors obtained in the band-structure calculation. Before the Raman transition, the momentum distribution of the $p_x \pm ip_y$ condensate is sharply peaked at K_1 and K_2 with a small distribution width Λ, and within this small region $\Omega(\mathbf{k})$ can be considered as a constant, estimated by $\Omega \approx 0.98\Omega_0$ for the typical value of the experimental parameters. So during the Raman transition, the small wave packets around K_1 and K_2 are transferred by the same formula without distortion. When we choose the duration of the Raman pulse as $\Omega\delta t = \pi/4$, the wave packets around K_1 and K_2 with $|d\mathbf{k}| \leqslant \Lambda$ are transferred by

$$C'_{\mathbf{K}_1+d\mathbf{k}} = (C_{\mathbf{K}_1+d\mathbf{k}} - ie^{i\phi}C_{\mathbf{K}_2+d\mathbf{k}})/\sqrt{2},$$

$$C'_{\mathbf{K}_2+d\mathbf{k}} = (C_{\mathbf{K}_2+d\mathbf{k}} - ie^{-i\phi}C_{\mathbf{K}_1+d\mathbf{k}})/\sqrt{2}. \qquad (6)$$

Right after these Raman pulses, we turn off the trapping optical potential and perform TOF imaging to measure the particle density distribution in momentum space around $\mathbf{K}_{1(2)}$. The density difference $\langle\delta n'(d\mathbf{k})\rangle \equiv \langle n'_{K_2+d\mathbf{k}} - n'_{K_1+d\mathbf{k}}\rangle = \langle C'^\dagger_{K_2+d\mathbf{k}}C'_{K_2+d\mathbf{k}} - C'^\dagger_{K_1+d\mathbf{k}}C'_{K_1+d\mathbf{k}}\rangle$ gives the of-diagonal correlation for the original BEC

$$\delta n'(d\mathbf{k}) = i\langle e^{i\phi}C^\dagger_{K_1+d\mathbf{k}}C_{K_2+d\mathbf{k}} - e^{-i\phi}C^\dagger_{K_2+d\mathbf{k}}C_{K_1+d\mathbf{k}}\rangle. \qquad (7)$$

Notice that the experimental observable $\delta n'(d\mathbf{k} =0)$, the height difference between the peaks in K_1 and K_2, is dependent on the phase difference of the two Raman pulses ϕ. For the $p_x \pm ip_y$ BEC, after the Raman pulse, we see that $\delta n'(d\mathbf{k} =0) \propto \cos\phi$ from Eq. (7). The oscillation of $\delta n'$ with ϕ indicates coherence of the two Raman pulses, which is critical to phase-sensitive detection. For $\phi = 0$, $\delta n'(d\mathbf{k} =0) = i\langle C^\dagger_{K_1}C_{K_2} - C^\dagger_{K_2}C_{K_1}\rangle$ represents the order parameter of the orbital ordering of the original UBEC.

With this phase-sensitive measurement, we can easily distinguish the complex condensate $|\Psi\rangle \propto \frac{1}{2^{N_c/2}\sqrt{N_c!}}(C^\dagger_{K_1} + e^{i\theta}C^\dagger_{K_2})^{N_c}|O\rangle$ and other plausible scenarios, such as the phase separation or incoherent mixing between the polar UBECs $|\Psi_1\rangle = \frac{1}{\sqrt{N_c!}}(C^\dagger_{K_1})^{N_c}|O\rangle$ and $|\Psi_2\rangle = \frac{1}{\sqrt{N_c!}}(C^\dagger_{K_2})^{N_c}|O\rangle$. In conventional TOF imaging, both of them exhibit four peaks with the same height thus cannot be distinguished. Under this phase-sensitive TOF imaging, we find that for the $p_x \pm ip_y$ UBEC, $\langle\Psi|n'_{K_2+d\mathbf{k}}|\Psi\rangle = 0$, which means that after Raman transition, the initial complex UBEC turns to the polar UBEC condensing only at K_1, and the predicted new TOF images are shown in Fig. 4(a) with only two peaks. However, for the incoherent mixing state between the condensates Ψ_1 and Ψ_2, after the Raman transition, the polar UBECs $\Psi_{1(2)}$ will turn to complex UBECs $\Psi'_{1(2)}$, each of which exhibits the four peaks with the same height in the TOF imaging; thus the incoherent mixing of them still preserves this four-peak imaging, as shown in Fig. 4(b).
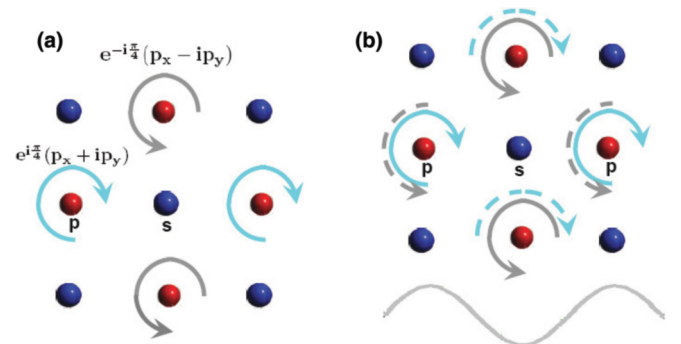

FIG. 5. (Color online) (a) Vortex-antivortex lattice structure of the $p_x \pm ip_y$ BEC before the Raman transition; (b) the real-space current pattern during the Raman transition, solid (dashed) arrows denote original (reflected) currents.

To get a better understanding of our results, we provide a real-space picture to illustrate the complex-real UBEC transition during the Raman process. Before the Raman transition, the $p_x \pm ip_y$ UBEC exhibits a vortex-antivortex lattice structure in the B sublattice (p-orbital sites), as shown in Fig. 5(a). The Raman beams introduce an extra potential with the form of Eq. (3), as shown in Fig. 5(b). Without loss of generality, we focus on one site in the B sublattice, initially the local wave function within this site can be approximately considered as $\varphi(\mathbf{r}) \sim e^{i\frac{\pi}{4}} [\varphi_x(\mathbf{r}) + i\varphi_y(\mathbf{r})]$, where $\varphi_{x(y)}(\mathbf{r})$ denote the $p_{x(y)}$-orbital Wannier function. During the Raman transition, the initial current is reflected by the extra potential, and the local wave function turns to $\varphi(t) = \cos(\Omega t)\varphi(\mathbf{r}) + \sin(\Omega t)\varphi^*(\mathbf{r})$, where $\varphi^*(\mathbf{r})$ is the TR counterpart of $\varphi(\mathbf{r})$ carrying a current with an opposite direction. Initially, $\varphi(0) = \varphi(\mathbf{r})$ denotes the $p_x + ip_y$ local state; at the momentum of $t_0\Omega = \pi/4$, the reflected current happens to cancel with the initial one, and it turns to a polar state with the real wave function $\varphi(t_0) \sim \varphi_x(\mathbf{r}) - \varphi_y(\mathbf{r})$, and the corresponding polar UBEC exhibits two peaks in the TOF spectrum, as shown in Fig. 4(a).

In above analysis of the Raman transition, we neglected the effect of interaction, which is responsible for the broadening of the TOF imaging peaks [26,27]. Now we estimate the interaction effect by solving the time evolution from the Gross-Pitaevskii (GP) equations (the GP equation gives an adequate description of the interaction since the initial state of the system is a BEC). A similar problem has been addressed for the many-body Rabi oscillation in a two-component BEC [28]. As analyzed above, we neglect the deformation of $\Psi_1(\mathbf{r})$ and $\Psi_2(\mathbf{r})$ during the time evolution, and the dynamics of the system can be approximately considered as a two-mode transition, thus the wave function during the time evolution can be expressed as $\Psi(t) = C_1(t)\Psi_1 + C_2(t)\Psi_2$. The corresponding GP equation reads

$$i\frac{\partial C_1(t)}{\partial t} = \Omega C_2 + (2g|C_1|^2 + 4g'|C_2|^2)C_1 + 2g'C_1^*C_2^2,$$

$$i\frac{\partial C_2(t)}{\partial t} = \Omega C_1 + (4g'|C_2|^2 + 2g|C_2|^2)C_2 + 2g'C_2^*C_1^2,$$

where $g = g_0\rho \int d^2r |\Psi_1(r)|^4 = g_0\rho \int d^2r |\Psi_2(r)|^4$, $g' = g_0\rho \int d^2r |\Psi_1(r)|^2 |\Psi_2(r)|^2$. ρ is the average density, g_0 is
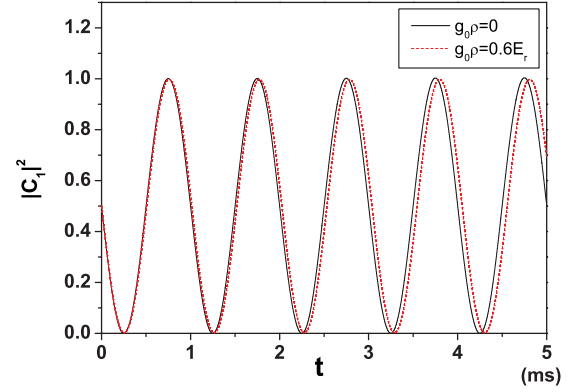

FIG. 6. (Color online) Time evolution of the fraction of bosons in K_1 with $\Omega = 2\pi \times 0.5$ kHz, $g_0\rho = 0$ (solid line) and $0.6E_r$ (dashed line).

the s-wave scattering interaction parameter. In the experiment [16], $g_0\rho$ is estimated to be $0.6E_r$. Using the initial condition $C_1(0) = 1/\sqrt{2}$, $C_2(0) = i/\sqrt{2}$ ($p_x + ip_y$ state), and $\Omega = 2\pi \times 0.5$ kHz, we get the time evolution of the fraction of bosons in the K_1 wave packet, and compare the result with the noninteracting case. As shown in Fig. 6, the interaction barely changes the Rabi oscillation within the duration of the Raman pulses in our case, which implies the single-particle Rabi oscillation approximation we adopted above provides an accurate description of the many-body dynamics of the system during the Raman transition.

To conclude, we propose a phase-sensitive detection scheme to identify the nontrivial symmetry of recently observed $p_x \pm ip_y$ orbital BECs, where the connection between different condensate momenta is built up by the momentum kick provided by impulsive Raman pulses. Our scheme can also be applied to the phase-sensitive detection for unconventional BECs with other symmetries, e.g., the recently observed BEC in f-orbital bands of the optical lattice [17].

[1] D. A. Wollman, D. J. Van Harlingen, W. C. Lee, D. M. Ginsberg, and A. J. Leggett, Phys. Rev. Lett. **71**, 2134 (1993).

[2] C. C. Tsuei, J. R. Kirtley, C. C. Chi, Lock See Yu-Jahnes, A. Gupta, T. Shaw, J. Z. Sun, and M. B. Ketchen, Phys. Rev. Lett. **73**, 593 (1994).

[3] A. J. Leggett, Rev. Mod. Phys. **47**, 331 (1975).

[4] K. Nelson, Z. Mao, Y. Maeno, and Y. Liu, Science **306**, 1151 (2004).

[5] F. Kidwingira, J. D. Strand, D. J. V. Harlingen, and Y. Maeno, Science **314**, 1267 (2006).

[6] C. Wu, Mod. Phys. Lett. B **23**, 1 (2009).

[7] Z. Cai and C. Wu, Phys. Rev. A **84**, 033635 (2011).

[8] A. Isacsson and S. M. Girvin, Phys. Rev. A **72**, 053604 (2005).

[9] W. V. Liu and C. Wu, Phys. Rev. A **74**, 013607 (2006).

[10] C. Wu, W. V. Liu, J. E. Moore, and S. Das Sarma, Phys. Rev. Lett. **97**, 190406 (2006).

[11] A. B. Kuklov, Phys. Rev. Lett. **97**, 110405 (2006).

[12] V. M. Stojanović, C. Wu, W. V. Liu, and S. Das Sarma, Phys. Rev. Lett. **101**, 125301 (2008).

[13] Q. Zhou, J. V. Porto, and S. Das Sarma, Phys. Rev. B **83**, 195106 (2011).

[14] X. P. Li, Z. X. Zhang and W. V. Liu, Phys. Rev. Lett. **108**, 175302 (2012).

[15] T. Müller, S. Fölling, A. Widera, and I. Bloch, Phys. Rev. Lett. **99**, 200405 (2007).

[16] G. Wirth, M. Ölschläger, and A. Hemmerich, Nat. Phys. **7**, 147 (2011).

[17] M. Ölschläger, G. Wirth, and A. Hemmerich, Phys. Rev. Lett. **106**, 015302 (2011).

[18] N. Y. Kim, K. Kusudo, C. Wu, N. Masumoto, C. Schneider, S. Höling, N. Kumada, L. Worschech, A. Forchel, and Y. Yamamoto, Nat. Phys. **7**, 681 (2011).

[19] R. P. Feynman, Statistical Mechanics, A Set of Lectures (Addison-Wesley, Boston, 1972).

[20] F. Dalfovo, S. Giorgini, L. P. Pitaevskii, and S. Stringari, Rev. Mod. Phys. **71**, 463 (1999).

[21] A. Hemmerich (unpublished).

[22] L.-M. Duan, Phys. Rev. Lett. **96**, 103201 (2006).

[23] S. Richard, F. Gerbier, J. H. Thywissen, M. Hugbart, P. Bouyer, and A. Aspect, Phys. Rev. Lett. **91**, 010405 (2003).

[24] D. Hellweg, L. Cacciapuoti, M. Kottke, T. Schulte, K. Sengstock, W. Ertmer, and J. J. Arlt, Phys. Rev. Lett. **91**, 010406 (2003).

[25] T. Kitagawa, A. Aspect, M. Greiner, and E. Demler, Phys. Rev. Lett. **106**, 115302 (2011).

[26] W. Yi, G.-D. Lin, and L.-M. Duan, Phys. Rev. A **76**, 031602 (2007).

[27] G.-D. Lin, W. Zhang, and L.-M. Duan, Phys. Rev. A **77**, 043626 (2008).

[28] H. Saito, R. G. Hulet, and M. Ueda, Phys. Rev. A **76**, 053619 (2007).